The Journal of Chemical Physics

The size and affinity effect of counterions on self-assembly of charged block copolymers

Cite as: J. Chem. Phys. **152**, 124901 (2020); https://doi.org/10.1063/5.0002896
Submitted: 28 January 2020 • Accepted: 06 March 2020 • Published Online: 24 March 2020

Jiadi Jiang, Xu Chen, Shuang Yang, et al.

The Journal of Chemical Physics ARTICLE scitation.org/journal/jcp

The size and affinity effect of counterions on self-assembly of charged block copolymers

Cite as: J. Chem. Phys. 152, 124901 (2020); doi: 10.1063/5.0002896
Submitted: 28 January 2020 • Accepted: 6 March 2020 •
Published Online: 24 March 2020

Jiadi Jiang, Xu Chen, Shuang Yang,[a] and Er-Qiang Chen

AFFILIATIONS

Beijing National Laboratory for Molecular Sciences, Department of Polymer Science and Engineering and Key Laboratory of Polymer Chemistry and Physics of Ministry of Education, College of Chemistry, Peking University, Beijing 100871, People's Republic of China

[a]Author to whom correspondence should be addressed: shuangyang@pku.edu.cn

ABSTRACT

The effect of counterions' size and affinity on the microphase separated morphologies of neutral-charged diblock copolymers is investigated systematically using a random phase approximation (RPA) and self-consistent field theory (SCFT). The phase diagrams as a function of χ_{AB} and f_A at different counterion sizes and different affinities to neutral blocks are constructed, respectively. Stability limits calculated using the RPA are in good agreement with the disorder-body-centered cubic phase boundaries from SCFT calculations. It was found that increasing the size of counterions causes the phase diagram to shift upward and leftward, which is attributed to electrostatic interactions and the intrinsic volume of counterions. The domain size of the ordered phase shows an unexpected tendency that it decreases with increasing counterions' size. The counterions' distributions in H and G phases demonstrate that it is electrostatic interaction, instead of packing frustration, that plays a leading role in such systems. For finite size counterions, with the increase in affinity between counterions and neutral blocks, the phase diagram shifts upward, indicating the improved compatibility between different blocks. Furthermore, the affinity effect between counterions and neutral blocks can be mapped into an effective Flory parameter $\chi'_{AB} = \chi_{AB} + 0.27\chi_{BC}$.

I. INTRODUCTION

Block copolymers can self-assemble into a variety of precisely controlled long-range ordered nanostructures due to the incompatibility between different blocks and the chain connectivity. It is a "bottom up" approach to design the material with special microdomains.[1] Depending on the composition, chain length, and incompatibility parameter, the typical self-assembled morphologies include lamellae (L), hexagonal cylinder (H), body-centered cubic (BCC), or bicontinuous gyroid (G) phase. Recently, the self-assembly of ion-containing block copolymers receives a great deal of attention due to the fact that their ion-embedded structures may have important potential applications in electrochemical energy storage and delivery devices as solid-state electrolytes or ion-conductive membranes[2,3] and nanolithography.[4] Neutral-charged block copolymers constitute of one main material, which include salt-doped copolymers[5–8] [such as polystyrene-b-poly(ethylene oxide)(PS-PEO)] as well as single-ion conducting block polyelectrolytes that are synthesized by connecting intrinsically charged blocks and neutral blocks.[9–13] While the former shows an intrinsic disadvantage of low lithium-ion transference number,[14,15] limited power delivery,[16] and the lithium dendrite growth during the recharge[17] due to the formation of a charge gradient, the latter one shows better conductivity and markedly improved mechanical strength.[12]

For all ion-containing block copolymers, the ion transport highly depends on their self-assembled morphology at the molecular level. For neutral-charged diblock copolymers, a typical model of single-ion conducting polyelectrolyte, a large number of intriguing nanodomain structures were observed, and the corresponding conductivity of such materials has also been studied.[18–21] Although significant progress on the experiments has been achieved, the effect of electrostatic interaction on morphology is still far from complete understanding. The factors such as translational entropy of counterions, solvation of charged units, strong correlations from charges, and counterion adsorption for highly charged blocks may play roles, which compete with conformational entropy of chains and incompatibility between different blocks.

Marko and Rabin first used a random phase approximation (RPA) analysis to investigate the order–disorder phase transition of neutral-charged diblock copolymers.[22,23] They revealed that the translational entropy of the counterions and electrostatic screening of added salts stabilize the disordered phase over the ordered phases. Kumar and Muthukumar studied the salt-free melts in the weak segregation limit using the RPA and Landau expansion, and they handled the lamellar morphology using self-consistent field theory (SCFT) based on the Poisson–Boltzmann equation.[24] The results show that the counterions tend to be located in the charged block-rich phase and the charging one of the blocks decreases the segregation strength effectively. Yang *et al.* extended the SCFT calculations to include complex H, G, or BCC phases and calculated the order–order phase transition (OOT) boundaries for the same system.[25] It was shown that different ordered phases are stabilized as a result of charging one of the blocks, which is qualitatively in agreement with the experiments of Balsara *et al.* Later, Wang *et al.* considered the dipolar feature of polar solvents and developed a SCFT to study the solvation effect in block polyelectrolytes.[26] Liu *et al.* calculated the phase behavior of a diblock polyelectrolyte in two-dimensional real space and solved the SCFT equations for L and H phases.[27]

The above theories only considered point-like ions/counterions and ignored the correlation effect. Goswami *et al.* carried out coarse grained molecular dynamic (MD) simulation to study charged diblock copolymer melts with explicit treatment of electrostatics. It was revealed that the charge aggregation and counterion adsorption in a low-dielectric condition play an important role in stabilizing ordered morphologies. Especially, charge agglomeration can lead to a percolated structure and a novel "inverse" morphology (a phase with a minority component constitutes the continuous matrix). The strong correlation from long range Coulomb interaction may be dominant in some cases. An important progress on this issue was made by Sing *et al.* They developed a complex approach called SCFT-LS theory that does not rely on the Poisson–Boltzmann equation; instead, they used Liquid State (LS) integral equation theory to deal with charge correlations in the nanoscale range.[28] When the polymer is highly charged, its calculated phase diagram shows a "chimney"-like regime, which means that even two fully compatible blocks may be microphase separated into ordered phases. They attributed this phenomenon to charge cohesion effect.[29,30] Recently, Zhai *et al.* studied the effect of charge fraction and dielectric constant on phase behavior using dissipative particle dynamics (DPD) simulations. It was found that the charge effect on the phase diagram in their simulation is between Yang *et al.*[25] and Sing *et al.*[29] Furthermore, they developed a novel "diffusivity tensor" approach to calculate the anisotropic degree in ion diffusivity and found the inverse topology gyroid and cylindrical phases are ideal candidates for solid-state electrolytes.[31] Besides, some theoretical works for lithium salt doping in PEO-like copolymer systems explicitly account for the association between the EO unit and lithium ion. Different aspects including the Born solvation energy,[32–36] the effect of dielectric inhomogeneity,[37] charge screening effects,[38] and ion correlation effects[39,40] on the thermodynamics have been highlighted.

The characteristic of counterions is ignored generally in theories. Nevertheless, a variety of experiments revealed that the counterions indeed have a nontrivial influence in determining the self-assembled structures of block polyelectrolytes.[6,9,41–45] For salt-doped PS-PEO copolymers, Young, Epps, and Thomas found that the different counterions alter the location of order–order phase transition boundaries during the addition of salt.[6] Loo *et al.* found that the dependence of domain spacing on the salt concentration was nonmonotonic in asymmetric Nock copolymer electrolytes, which cannot be solely accounted for by using the Born solvation energy concept.[46,47] In a recent experiment, Wang *et al.* found that for neutral-charged diblock copolymers with lower disorder-to-order transition phase behavior, increasing counterion size and salt content shifts the disorder-to-order transition temperature to higher temperature.[44] Apparently, the counterion with finite size will expand the effective volume fraction of charged blocks. However, the concrete role of counterions on determining the morphology of charged block copolymers remains an unclear feature. In this paper, we use RPA and SCFT to theoretically investigate the influence of counterion characters on the phase behavior of neutral-charged diblock copolymer melts. We first analyze the effect of counterions' size on the phase diagram and the domain size. Then, we calculate the concentration distribution of all species in one specific phase to focus on the role of counterions in it. Finally, inspired by the idea that promoting charge dissociation can enhance the ionic conductivity in single-ion conducting systems,[9] we apply different affinities of counterions to two blocks to discover its effect on the phase diagram. These results provide a basis about the role that counterions play in the self-assembly of ion-containing block polyelectrolytes.

II. THEORETICAL MODEL

We consider a system of volume V consisted of n_p charged linear diblock copolymers as well as small ions (only counterions are considered in this study). The copolymers are modeled as continuous Gaussian chains having an equal degree of polymerization of N and composed of two bead species (we denote by labels A and B). The A block is positive charged, and the negative counterions are dissociated from it. We use label C to represent counterions. The B block is a neutral part. We assume that the charges are uniformly distributed along A block's backbone and use z_A to represent the degree of ionization (we call it as charge fraction). This homogeneous charge density along the backbone is valid when z_A is relatively low. The monomer volumes of A and B, and the volume of counterions are denoted by v_A, v_B and v_C, respectively. b_A and b_B are used to represent the Kuhn lengths of A and B monomers. For simplicity, we assume $b_A = b_B = b$. The degrees of polymerization for A and B blocks are N_A and N_B, respectively. The fractional compositions of block A is then given by $f_A = N_A/N$. The valence of counterions is denoted by z_C. The total number of counterions is set as $n_C = -z_A n_p N_A/z_C$ to ensure electric neutrality.

The microscopic concentrations of A, B, and C in position r are given by

$$\hat{\rho}_\alpha(\mathrm{r}) = \sum_{i=1}^{n_p} \int_0^{N_\alpha} \mathrm{d}s\delta(\mathrm{r} - \mathrm{R}_i^\alpha(s)), \tag{1}$$

$$\hat{\rho}_C(\mathrm{r}) = \sum_{i=1}^{n_C} \delta(\mathrm{r} - \mathrm{r}_i^C), \tag{2}$$

where $\alpha = A, B$. $\mathrm{R}_i^{\alpha}(s)$ represents the position of the sth monomer at α-block of the ith polymer chain. r_i^C denotes the position of the ith counterion.

The Edwards Hamiltonian of the system is the sum of three contributions, $H = H_{ela} + H_{int} + H_{ele}$. H_{ela} is the elastic energy due to stretching of the polymer chains and can be written as

$$H_{ela} = \sum_{\alpha=A,B} \sum_{i=1}^{n_p} \frac{3}{2b^2} \int_0^{N_\alpha} \mathrm{d}s \left(\frac{\mathrm{d}\mathrm{R}_i^{\alpha}(s)}{\mathrm{d}s} \right)^2. \tag{3}$$

H_{int} is the incompatibility part of the interaction energy and has the form

$$H_{int} = \int \mathrm{d}\mathrm{r}[\chi_{AB} v_A v_B \hat{\rho}_A(\mathrm{r}) \hat{\rho}_B(\mathrm{r}) + \chi_{BC} v_B v_C \hat{\rho}_B(\mathrm{r}) \hat{\rho}_C(\mathrm{r}) + \chi_{AC} v_A v_C \hat{\rho}_A(\mathrm{r}) \hat{\rho}_C(\mathrm{r})], \tag{4}$$

where χ_{AB}, χ_{BC}, and χ_{AC} are the Flory–Huggins interaction parameters between A and B, B and C, A and C, respectively.

H_{ele} is the electrostatic contribution and can be written as

$$H_{ele} = \int \mathrm{d}\mathrm{r} \left(\beta e \psi(\mathrm{r}) \hat{\rho}_e(\mathrm{r}) - \frac{1}{2} \beta \varepsilon |\nabla \psi(\mathrm{r})|^2 \right), \tag{5}$$

where β is equal to $1/k_B T$. e is the elementary charge, and $\psi(\mathrm{r})$ is the electrostatic potential. $\hat{\rho}_e(\mathrm{r})$ is the charge density at position r and can be represented as $\hat{\rho}_e(\mathrm{r}) = z_A \hat{\rho}_A(\mathrm{r}) + z_C \hat{\rho}_C(\mathrm{r})$. ε is the dielectric constant, which is assumed to be spatial invariant in our model. In fact, the non-uniform distribution of dielectric constant may have an important consequence on the morphologies. For example, the preferential solvation energy of anions in domains with higher dielectric permittivity may provide a large driving force for microphase separation.[33,34] de Pablo *et al.* developed a Green's function method by solving Poisson's equation and found that the non-uniform dielectric constant leads to a significant influence on the density profiles of different blocks as well as the phase diagram.[37] Cascella *et al.* proposed a good route to handle the electrostatic interactions with inhomogeneous dielectric screening in which a density functional-based formalism was used[48] in combination with the hybrid particle field method coupled to molecular dynamics.[40,49] However, here we ignore this complexity of ε and concentrate on the counterion size effect. When the A and B blocks have the similar dielectric constant, the solvation energy may be unimportant and our model is applicable.

The canonical partition function then can be written in terms of the functional integral over all the chain conformations and counterion positions,

$$Z = \frac{\zeta}{n_p! n_C!} \int \mathrm{D}\{\mathrm{R}(s)\} \mathrm{D}\{\mathrm{r}_C\} \mathrm{D}\{\psi\} \prod_{\mathrm{r}} \delta(\hat{\rho}_A(\mathrm{r}) v_A + \hat{\rho}_B(\mathrm{r}) v_B + \hat{\rho}_C(\mathrm{r}) v_C - 1) \prod_{i=1}^{n_p} \delta\left(\mathrm{R}_i^A(N_A) - \mathrm{R}_i^B(N_B)\right) \exp(-H). \tag{6}$$

Here, ζ is the contribution due to the kinetic energy and is constant in this system. The first Dirac delta function represents the incompressibility condition at each position for our system. The second delta function ensures the chain connectivity between A and B blocks.

A. Random phase approximation (RPA)

One can use the RPA to do a linear response treatment for a homogeneous system near the stability limit.[50,51] By expanding the free energy expression of the inhomogeneous phase around the homogeneous phase to the second order of the densities,[24]

$$F = F_0 + \delta F + O(\rho^3). \tag{7}$$

The second term in ρ^2 has the form of

$$\delta F = \frac{1}{2} \int \frac{\mathrm{d}^3 q}{(2\pi)^3} \boldsymbol{\rho}(\boldsymbol{q}) \boldsymbol{S}^{-1} \boldsymbol{\rho}^T(-\boldsymbol{q}). \tag{8}$$

$\boldsymbol{\rho}(\boldsymbol{q})$ is the vector of density for each species, and $\boldsymbol{S}$ is the structure matrix. In the RPA, $\boldsymbol{S}$ is given by

$$\boldsymbol{S}^{-1} = \boldsymbol{S}^{0^{-1}} + \boldsymbol{W} + \boldsymbol{U}(\boldsymbol{q}), \tag{9}$$

where

$$\boldsymbol{S}^0 = \begin{pmatrix} S^0_{\mathrm{AA}} & S^0_{\mathrm{AB}} & 0 \\ S^0_{\mathrm{AB}} & S^0_{\mathrm{BB}} & 0 \\ 0 & 0 & S^0_{\mathrm{CC}} \end{pmatrix},$$

$$\boldsymbol{W} = \begin{pmatrix} 0 & v_{\mathrm{A}} v_{\mathrm{B}} \chi_{\mathrm{AB}} & v_{\mathrm{A}} v_{\mathrm{C}} \chi_{\mathrm{AC}} \\ v_{\mathrm{A}} v_{\mathrm{B}} \chi_{\mathrm{AB}} & 0 & v_{\mathrm{B}} v_{\mathrm{C}} \chi_{\mathrm{BC}} \\ v_{\mathrm{A}} v_{\mathrm{C}} \chi_{\mathrm{AC}} & v_{\mathrm{B}} v_{\mathrm{C}} \chi_{\mathrm{BC}} & 0 \end{pmatrix},$$

$$\boldsymbol{U}(\boldsymbol{q}) = \begin{pmatrix} z_{\mathrm{A}}^2 u(\boldsymbol{q}) & 0 & z_{\mathrm{A}} z_{\mathrm{C}} u(\boldsymbol{q}) \\ 0 & 0 & 0 \\ z_{\mathrm{A}} z_{\mathrm{C}} u(\boldsymbol{q}) & 0 & z_{\mathrm{C}}^2 u(\boldsymbol{q}) \end{pmatrix}.$$

The S^0_{ab} denotes the bare structure factor. For ideal Gaussian chains, the structure factors take the form

$$S^0_{\mathrm{AA}} = N(\rho^0_{\mathrm{A}} + \rho^0_{\mathrm{B}}) g(f_A, x),$$
$$S^0_{\mathrm{BB}} = N(\rho^0_{\mathrm{A}} + \rho^0_{\mathrm{B}}) g(1 - f_A, x),$$
$$S^0_{\mathrm{AB}} = N(\rho^0_{\mathrm{A}} + \rho^0_{\mathrm{B}}) [g(1, x) - g(f_A, x) - g(1 - f_A, x)]/2,$$
$$S^0_{\mathrm{CC}} = \rho^0_{\mathrm{C}},$$

where ρ^0_{A}, ρ^0_{A}, and ρ^0_{A} are the averaged densities of A monomer, B monomer, and counterion C, respectively. $g(f, x)$ is the Debye function

$$g(f, x) = 2[fx + \exp(-fx) - 1]/x^2,$$

where $x = R_g^2 q^2$, and $R_g = (N/6)^{1/2} b$ is the radius of gyration for the ideal Gaussian chain. In matrix $\boldsymbol{U}(\boldsymbol{q})$, the term $u(\boldsymbol{q})$ denotes the electrostatic potential in Fourier space as

$$u(\boldsymbol{q}) = \frac{4\pi l_b}{q^2}. \tag{10}$$

Here, l_B is the Bjerrum length $l_B = e^2/4\pi\varepsilon k_B T$. Thus, the structure matrix can be written as

$$\boldsymbol{S}^{-1} \equiv \begin{pmatrix} T_{AA} & T_{AB} & T_{AC} \\ T_{AB} & T_{BB} & T_{BC} \\ T_{AC} & T_{BC} & T_{CC} \end{pmatrix} = \begin{pmatrix} \frac{S^0_{BB}}{S^0_{AA}S^0_{BB}-S^{0\,2}_{AB}} + z_A^2 u(\boldsymbol{q}) & -\frac{S^0_{AB}}{S^0_{AA}S^0_{BB}-S^{0\,2}_{AB}} + \nu_A\nu_B\chi_{AB} & \nu_A\nu_C\chi_{AC} + z_Az_Cu(\boldsymbol{q}) \\ -\frac{S^0_{AB}}{S^0_{AA}S^0_{BB}-S^{0\,2}_{AB}} + \nu_A\nu_B\chi_{AB} & \frac{S^0_{AA}}{S^0_{AA}S^0_{BB}-S^{0\,2}_{AB}} & \nu_B\nu_C\chi_{BC} \\ \nu_A\nu_C\chi_{AC} + z_Az_Cu(\boldsymbol{q}) & \nu_B\nu_C\chi_{BC} & \frac{1}{S^0_{CC}} + z_C^2u(\boldsymbol{q}) \end{pmatrix}. \tag{11}$$

Then, we take the incompressibility requirement into account, which means in Fourier space we have (for $\boldsymbol{q} \neq 0$)

$$\nu_A\rho_A(\boldsymbol{q}) + \nu_B\rho_B(\boldsymbol{q}) + \nu_C\rho_C(\boldsymbol{q}) = 0. \tag{12}$$

Thus, the term ρ_B in Eq. (8) can be substituted by

$$\rho_B(\boldsymbol{q}) = -\frac{\nu_A\rho_A(\boldsymbol{q}) + \nu_C\rho_C(\boldsymbol{q})}{\nu_B}. \tag{13}$$

The 3 × 3 structure matrix can then be simplified to the 2 × 2 structure matrix in the form of

$$\boldsymbol{S'}^{-1} = \begin{pmatrix} T_{AA} - \frac{2\nu_A}{\nu_B}T_{AB} + \frac{\nu_A^2}{\nu_B^2}T_{BB} & T_{AC} - \frac{\nu_C}{\nu_B}T_{AB} - \frac{\nu_A}{\nu_B}T_{BC} + \frac{\nu_A\nu_C}{\nu_B^2}T_{BB} \\ T_{AC} - \frac{\nu_C}{\nu_B}T_{AB} - \frac{\nu_A}{\nu_B}T_{BC} + \frac{\nu_A\nu_C}{\nu_B^2}T_{BB} & T_{CC} - \frac{2\nu_C}{\nu_B}T_{BC} + \frac{\nu_C^2}{\nu_B^2}T_{BB} \end{pmatrix}. \tag{14}$$

The order–disorder phase transition occurs when the eigenvalue of the matrix $\boldsymbol{S'}$ is divergent at some q^*. Therefore, the stability limit is calculated using $\det(\boldsymbol{S'}^{-1}(\boldsymbol{q})) = 0$.

B. Self-consistent field theory (SCFT)

Following the standard method of SCFT,[52,53] the free energy can be obtained from the partition function in Eq. (6). A detailed description of SCFT refers to Ref. 52. The resulting free energy functional is given by

$$\begin{aligned} \beta F = \int \mathrm{d}\mathbf{r}\Big[&- \sum_j \omega_j(\mathbf{r})\rho_j(\mathbf{r}) + \chi_{AB}\nu_A\nu_B\rho_A(\mathbf{r})\rho_B(\mathbf{r}) \\ &+ \chi_{BC}\nu_B\nu_C\rho_B(\mathbf{r})\rho_C(\mathbf{r}) + \chi_{AC}\nu_A\nu_C\rho_A(\mathbf{r})\rho_C(\mathbf{r}) + \beta e\psi(\mathbf{r})\rho_e(\mathbf{r}) \\ &- \frac{1}{2}\beta\varepsilon|\nabla\psi(\mathbf{r})|^2 + \eta(\mathbf{r})(\rho_A(\mathbf{r})\nu_A + \rho_B(\mathbf{r})\nu_B + \rho_C(\mathbf{r})\nu_C - 1)\Big] \\ &- n_p\ln(VQ_p) + \ln(n_p!) - n_C\ln(VQ_C) + \ln(n_C!). \end{aligned} \tag{15}$$

Here, β is the inverse of kT. j represents all species in the system including monomers A, B and counterion C. ρ_j is the density field of specie j, and ω_j is the corresponding conjugated field. η is a Lagrangian multiplier to ensure the incompressibility condition. Q_p and Q_C are the single molecule partition functions for a copolymer chain and a counterion in the external field, respectively. They have the following expressions:

$$Q_p = \frac{1}{V}\int \mathrm{D}\{\mathrm{R}(s)\}\exp\{-H_{cop}\}\delta(\mathrm{R}_i^A(N_A) - \mathrm{R}_i^B(N_B)), \tag{16}$$

$$Q_C = \frac{1}{V}\int \mathrm{d}\mathbf{r}\exp\{-\omega_C(\mathbf{r})\}, \tag{17}$$

where H_{cop} satisfies

$$H_{cop} = \sum_{\alpha=A,B}\int_0^{N_\alpha}\mathrm{d}s\left[\frac{3}{2b^2}\left(\frac{\mathrm{dR}^\alpha(s)}{\mathrm{d}s}\right)^2 + \omega_\alpha(\mathrm{R}^\alpha(s))\right]. \tag{18}$$

By using the saddle approximation and taking functional derivatives of βF with respect to ρ_j, ω_j, η, and ψ, the SCF equations can be obtained,

$$\omega_A(\mathbf{r}) = \chi_{AB}\nu_A\nu_B\rho_B(\mathbf{r}) + \chi_{AC}\nu_A\nu_C\rho_C(\mathbf{r}) + z_A\beta e\psi(\mathbf{r}) + \nu_A\eta(\mathbf{r}), \tag{19}$$

$$\omega_B(\mathbf{r}) = \chi_{AB}\nu_A\nu_B\rho_A(\mathbf{r}) + \chi_{BC}\nu_B\nu_C\rho_C(\mathbf{r}) + \nu_B\eta(\mathbf{r}), \tag{20}$$

$$\omega_C(\mathbf{r}) = \chi_{AC}\nu_A\nu_C\rho_A(\mathbf{r}) + \chi_{BC}\nu_B\nu_C\rho_B(\mathbf{r}) + z_C\beta e\psi(\mathbf{r}) + \nu_C\eta(\mathbf{r}), \tag{21}$$

$$\rho_A(\mathbf{r}) = \frac{n_p}{VQ_p}\int_0^{N_A}\mathrm{d}s q_A(\mathbf{r},s)q_A^+(\mathbf{r},N_A-s), \tag{22}$$

$$\rho_B(\mathbf{r}) = \frac{n_p}{VQ_p}\int_0^{N_B}\mathrm{d}s q_B(\mathbf{r},s)q_B^+(\mathbf{r},N_B-s), \tag{23}$$

$$\rho_C(\mathbf{r}) = \frac{n_C}{VQ_C}\exp(-\omega_C(\mathbf{r})), \tag{24}$$

$$\rho_A(\mathbf{r})\nu_A + \rho_B(\mathbf{r})\nu_B + \rho_C(\mathbf{r})\nu_C = 1, \tag{25}$$

$$\beta e\nabla^2\psi(\mathbf{r}) + 4\pi l_B\rho_e(\mathbf{r}) = 0, \tag{26}$$

$$\rho_e(\mathbf{r}) = z_A\rho_A(\mathbf{r}) + z_C\rho_C(\mathbf{r}). \tag{27}$$

In Eq. (22), $q_A(\mathbf{r}, s)$ is the A-chain propagator and defined as the probability of finding the end monomer of A block of length s at

point r with a free initial monomer. $q_A^+(\mathrm{r},s)$ is the probability of finding the end monomer of the A chain of length s at r, while the other end of the A chain is connected to the whole B block.[25] $q_B(\mathrm{r},s)$ and $q_B^+(\mathrm{r},s)$ have a similar definition. $q_\alpha(\mathrm{r},s)$ and $q_\alpha^+(\mathrm{r},s)$ ($\alpha = A, B$) satisfy the modified diffusion equations

$$\frac{\partial q_\alpha(\mathrm{r},s)}{\partial s} = \frac{b^2}{6}\nabla^2 q_\alpha(\mathrm{r},s) - \omega_\alpha(\mathrm{r})q_\alpha(\mathrm{r},s), \tag{28}$$

$$\frac{\partial q_\alpha^+(\mathrm{r},s)}{\partial s} = \frac{b^2}{6}\nabla^2 q_\alpha^+(\mathrm{r},s) - \omega_\alpha(\mathrm{r})q_\alpha^+(\mathrm{r},s) \tag{29}$$

with the initial condition

$$q_A(\mathrm{r},0) = 1, \quad q_B(\mathrm{r},0) = 1, \tag{30}$$

$$q_A^+(\mathrm{r},0) = q_B(\mathrm{r},N_B), \quad q_B^+(\mathrm{r},0) = q_A(\mathrm{r},N_A). \tag{31}$$

Q_p can then be simply calculated by

$$Q_p = \frac{1}{V}\int d\mathrm{r} q_\alpha^+(\mathrm{r},N_\alpha). \tag{32}$$

For a given set of parameters, Eqs. (12)–(22) constitute a closed set of self-consistent equations that generally needs to be solved numerically. We finally use the reciprocal-space method developed by Matsen and Schick[54] to solve them. The merit of the reciprocal-space method is that the partial differential equation is mapped into a set of linear equations, which simplify the solution considerably. Especially, the Poisson–Boltzmann equation (19) relating the coupling between long range electrostatic interaction and polymer conformation is easy to handle since we adopt uniform dielectric constant assumption. It is noted that the modified diffusion equations (21) and (22) will become a set of coupled first order stiff equations. Here, we use a more convenient and rapid solution, i.e., the fourth order Runge–Kutta method,[55] to solve the equations, instead of expanding the propagators in terms of the eigenvalues and eigenfunctions of the operator $b^2\nabla^2/6 - \omega_\alpha(\mathrm{r})$. Moreover, we use the Anderson mixing method to accelerate the iterative convergence step.[56–58] For a specified ordered phase with the given domain spacing D, one can obtain the free energy density after solving the SCF equations. The strategy to determine the most favorable phase is as follows: With the given systematic parameters (the χ parameter, chain length N, composition f_A, charge fraction z_A, and counterion size v_C), we calculate the minimized free energy density with respect to domain spacing D for each probe ordered phase. Then, we compare the free energy densities for different phase structures and choose the lowest one as the equilibrium phase structure under this condition. The phase structures we considered in this article include disorder phase (D), L phase, G phase, H phase, and BCC (or B) phase, as well as the block-A-rich inverse counterparts.

III. RESULTS AND DISCUSSIONS

Since our focus is the effect of counterion size and its affinity, for simplicity, we assume that counterions are monovalent and set $z_C = -1.0$. We set b as the length unit. The other parameters are chosen as follows: $N = 100$, $v_A = v_B = b^3 = 1.0$, $z_A = 0.1$, and $l_B = 4.0$. These parameters are fixed in this article. Other parameters, including χ_{AB}, χ_{AC}, χ_{BC}, f_A, and v_C, are changeable.

A. Size effect of counterions

In order to reveal the effect of counterion size on the morphology of neutral-charged block copolymer melts, here we ignore the affinity of counterions to two different blocks and set $\chi_{AC} = \chi_{BC} = 0.0$ for simplicity. The size of counterions, that is, v_C, is varied from 0.0 to 3.0.

1. Phase diagram with different counterions' size

The stability limits (dashed lines) of block copolymer salt-free melts are displayed in Fig. 1(a) for complete neutral one (black) and neutral-charged one with $v_C = 0$ (red) and $v_C = 3$ (blue). This is in agreement with the concept that effective miscibility between two blocks increase with the ionization of one block.[23] It is also found that the increase in counterion size leads to higher miscibility. The stability limits from the RPA are in good agreement with the order-disorder transition (ODT) boundaries (solid curves) predicted by SCFT. Next, we plot the OOT boundaries of the neutral-charged diblock copolymer in $\chi_{AB}N$ vs f_A parameter space. As shown in Fig. 1(b), the charged systems display the same microphases as well as the similar phase transition order to its neutral counterpart.[59] For the case of $v_C = 0$, an obvious difference is that the phase diagram exhibits upward and rightward shifts compared with the complete neutral one. This is due to the asymmetry between two blocks after the introduction of electrostatic charge on A blocks. The location of critical point shifts up to $\chi_{AB}N = 30$, $f_A = 0.6$ for the charged diblock copolymer with $z_A = 0.1$. The decreased immiscibility arising from the charged A block results from the increasing translational entropy effect of counterions as mentioned before.[25] Furthermore, the tendency of shift is more remarkable in low $\chi_{AB}N$ value than that in high $\chi_{AB}N$ value since the role of electrostatic interaction becomes weaker for stronger incompatible interaction (high $\chi_{AB}N$ value). Another important issue should be noted. Near the critical point, SCFT predicts a direct transition from disorder phase to H phase (or L phase) upon increasing $\chi_{AB}N$ without passing through BCC phase over a large composition range (0.4 ~ 0.6) for neutral systems. The same phenomenon occurs for H to L phase transition. Once the charges enter, the absence of middle phase (G or BCC) between ODT or OOT only occurs within a narrow range.

By increasing the size of counterions, the diagram has an upward and leftward shift, as shown in Fig. 1(b). We attribute this phenomenon to the electrostatic interactions between charged A blocks and counterions and the excluded volume effect of counterions. On the one hand, the counterions will mainly bind to A blocks and concentrate in A-rich domains due to the strong electrostatic attractions. Such enrichment increases the effective volume fraction of A-rich domains and causes the OOT boundaries to shift leftward. In other words, the actual composition of A blocks required to form a particular phase is reduced due to such concentration. On the other hand, the upward movement of the phase diagram results from two aspects. The first one is the counterion dilution effect. Both the concentrations of A and B monomers are reduced with increasing the counterions' size, considering that there are still a small part of counterions staying in the B-rich phase. This dilution effectively reduces the immiscible contacts between A and B monomers as well as the interfacial tension. The second one comes from the translational entropy of counterions. The bigger the

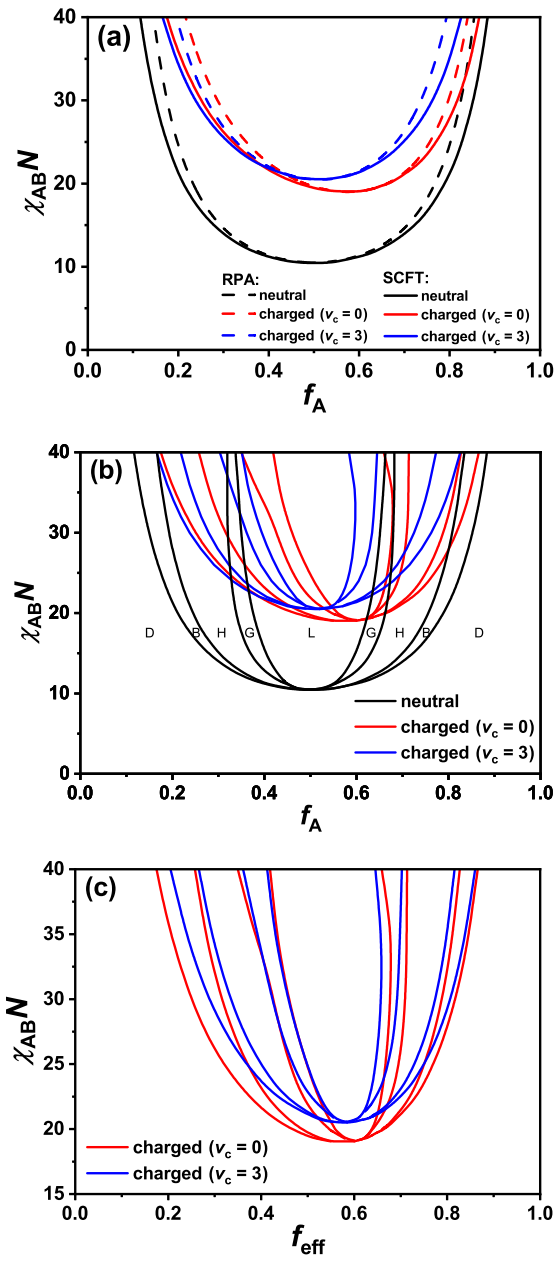

FIG. 1. (a) Phase diagram of neutral-charged diblock copolymer as a function of χ_{AB} and f_A. The solid curves are the disorder-BCC phase boundaries calculated by use of SCFT, while the dashed curves are the stability limit calculated by use of the RPA. Black curves correspond to neutral diblock copolymers, red curves is for the charged system with $v_C = 0$ and blue curves is for the charged system with $v_C = 3$. (b) Phase diagram with ordered phases for the neutral or charged system. (c) Phase diagram with ordered phases as a function of χ_{AB} and f_{eff}.

counterions, the larger the entropic loss to limit the counterions in A domains. We will address this issue later. Thus, a much higher value of χ_{AB} is needed to promote microphase separation. However, we emphasize that counterion size effects cannot be summarized solely by the effective volume fraction of the charged regions. In Fig. 1(c), we display the corrected phase diagram of the charged system with $v_C = 3$ (blue curve) in Fig. 1(b) by use of the effective composition of A-blocks f_{eff}, which is the total volume fraction of A monomers and counterions. It shows that the leftward shift of OOT transition boundaries can be accounted for to a large extent after the correction by use of the effective volume fraction of A blocks/counterions. The corrected transition boundaries have the tendency to move toward the central region (L phase). Even though, the ODT boundaries are different due to the counterion-induced dilution effect. The immiscibility between the A-rich region and B-rich region should be smaller than, namely, χ_{AB}. Therefore, the corrected phase diagram (blue curves) has an obvious upward shift compared with the system with point-like counterions (red curves).

A quantitative comparison between our prediction and experiments is difficult. Our SCF treatment does not account for the ion cohesion energy (electrostatic correlations) or solvation energy; however, our calculation still accounts for the isolated counterion effect and find some qualitative agreement with some experimental or simulation result. For the experiments about strongly interacting neutral-charged block copolymers, it is found that increasing counterions' size leads to higher threshold molecular weight for the appearance of the ordered phase, i.e., shifts the disorder-to-order transition to higher temperature.[44] In those systems, a higher temperature corresponds to a larger $\chi_{AB}N$ value. Although the authors argued that a bigger counterion leads to smaller ion cohesion energy and solvation energy, we believe that the size effect of the counterion indeed plays an important role.

2. Effect of counterions's size on domain size

In order to reveal the counterion size effect on the domain size, in Fig. 2(a), we give the domain size D of L phase as a function of interaction parameter $\chi_{AB}N$ at $f_A = 0.6$ at different excluded volume V_c. D value increases monotonically with increasing χ_{AB} at each v_C. Since our system is the weak segregation regime, the common scaling relationship $D \sim \chi_{AB}^{\mu}$, where the component μ ranges from 1/6 to 1/3 for a strong or intermediate segregation regime, is not held here. In fact, we do not find a simple scaling relationship between D and χ_{AB}. For the weak segregation regime with lower value of χ_{AB}, the domain spacing will decrease with decreasing v_C. This is a reasonable result because of the decrease in effective incompatibility between A-rich and B-rich domains, which comes from the dilution effect of larger counterions for A blocks. However, at high χ_{AB}, the domain spacing is almost independent of v_C. In a related study,[6] the authors found that for a lithium salt doping PEO-containing block copolymers, at any doping level, the domain spacing of the $LiClO_4$-doped system (smaller counterions) is always higher than that of the $LiCF_3SO_3$-doped system (larger counterions). This result should be explained only by counterion size effect, as shown by our calculation.

Figure 2(b) gives the principal domain spacing D^* of the ordered structures as a function of composition f_A at fixed $\chi_{AB}N = 30$. D^* is the nearest-neighbor distance between two domain layers, and it is related to the principal wave vector q^* through $D^* = 2\pi/q^*$. The discontinuous jumps in D^* correspond to the transitions between different ordered phases. In a neutral diblock system,

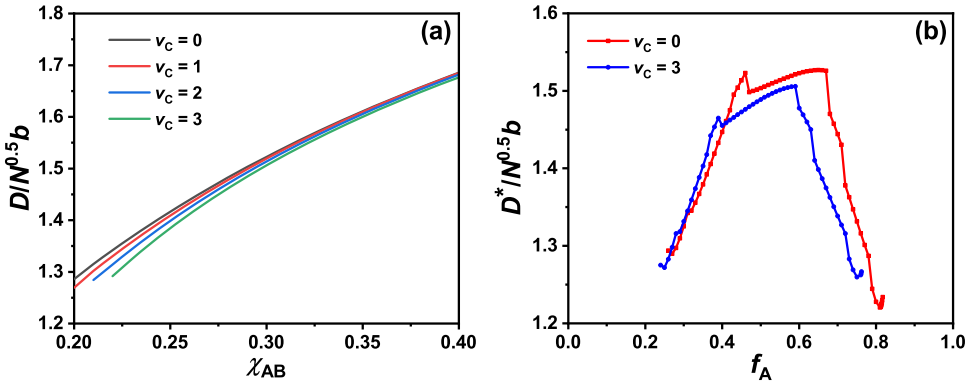

FIG. 2. (a) Domain spacing D^* of L phase as a function of the degree of segregation $\chi_{AB}N$ at $f_A = 0.6$. (b) Principal domain size D^* as a function of composition f_A at $\chi_{AB}N = 30$. The red curve corresponds to point-like counterions, and the blue curve is for counterions with large size of $v_c = 3$. D is the lattice size, and D^* is the nearest-neighbor distance between two domain layers. For L phase, $D = D^*$; for G phase, $D = 6^{1/2}D^*$; for H phase, $D = (\frac{4}{3})^{1/2}D^*$; and for B phase, $D = 2^{1/2}D^*$. The discontinuous jumps in D^* correspond to the transitions between different ordered phases.

the relationship between D^* and f_A is symmetrical.[60] The introduction of charges on A blocks leads to the asymmetry. The D^* value shifts leftward with increasing v_C, which is in accordance with the shift of the phase diagram. One can see that the domain spacing of L phase is an increasing function of f_A, while it is almost independent of the composition for neutral diblock copolymers.[60] Furthermore, D^* shows that the increase in counterion size may result in strong variation in q^* for a fixed f_A as a consequence of phase transition.

3. Concentration distribution and interface width of L phase

We calculate the interfacial width W of L phase between A and B domains to see the counterion size effect on the degree of segregation. The definition of interfacial width W is shown in Fig. 3(a). First, we find the minimum and the maximum values of A concentration (ρ_A^L and ρ_A^H) and draw the horizontal lines corresponding to the maximum and minimum (the black lines). Then, we find the interface between domains at which location the concentration of A monomers is equal to $(\rho_A^L + \rho_A^L)/2$. We further calculate the slope of concentration at the interface $d\rho_A/dx$ and draw the tangent (the red line). As shown in Fig. 3(a), the horizontal distance between two intersection points between red lines and two black lines is identified as the interface width W. Figure 3(b) gives W as a function of v_C at different incompatibility in an $f_A = 0.5$ copolymer melt. For each fixed χ_{AB}, a linear dependence between W/D and v_C is found, but the slope is larger for weaker incompatibility.

To understand how counterion size affects the segregation, we examine distributions of monomer A (ρ_A), charges on A blocks ($z_A\rho_A$), and counterions (ρ_C) in an $f_A = 0.5$ L phase with parameters $\chi_{AB} = 0.3$ in Fig. 4, where x is the coordinate normal to the lamella layer. With increasing counterion size, the concentration of monomer A in A-rich regions decreases significantly, while the distribution of monomer B is almost unchanged. Furthermore, counterions are mainly concentrated in the A-rich region due to the electrostatic interaction, and the total positive charges of monomer A in the A-rich region are compensated by negative charges carried by counterions to a large extent. The counterions tend to be concentrated on the central part of the A-rich region. However, the noncoincidence of two profiles ($z_A\rho_A$ and ρ_C) also indicates that there are net charges all over the system. The A-rich region has net positive charges, while the B-rich region has net negative charges.

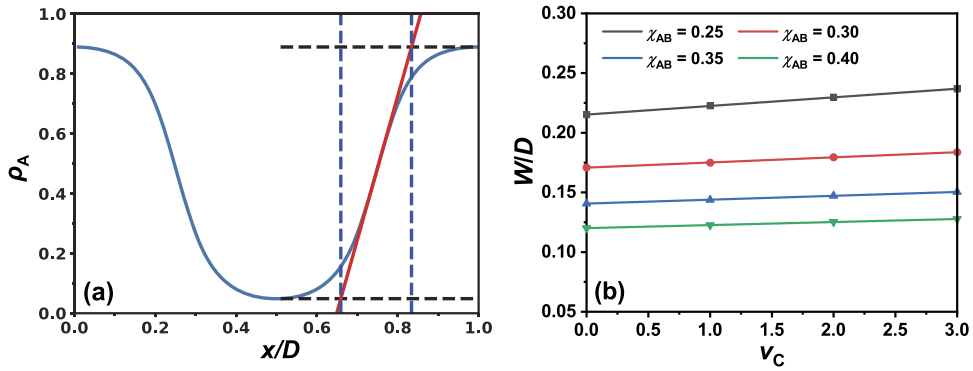

FIG. 3. (a) Calculation example for interface width with parameters $v_C = 1$, $f_A = 0.5$, and $\chi_{AB} = 0.30$. (b) Interface width W as a function of counterions' size v_C at different χ_{AB} values. A good linear relation between W/D and v_C is always observed.

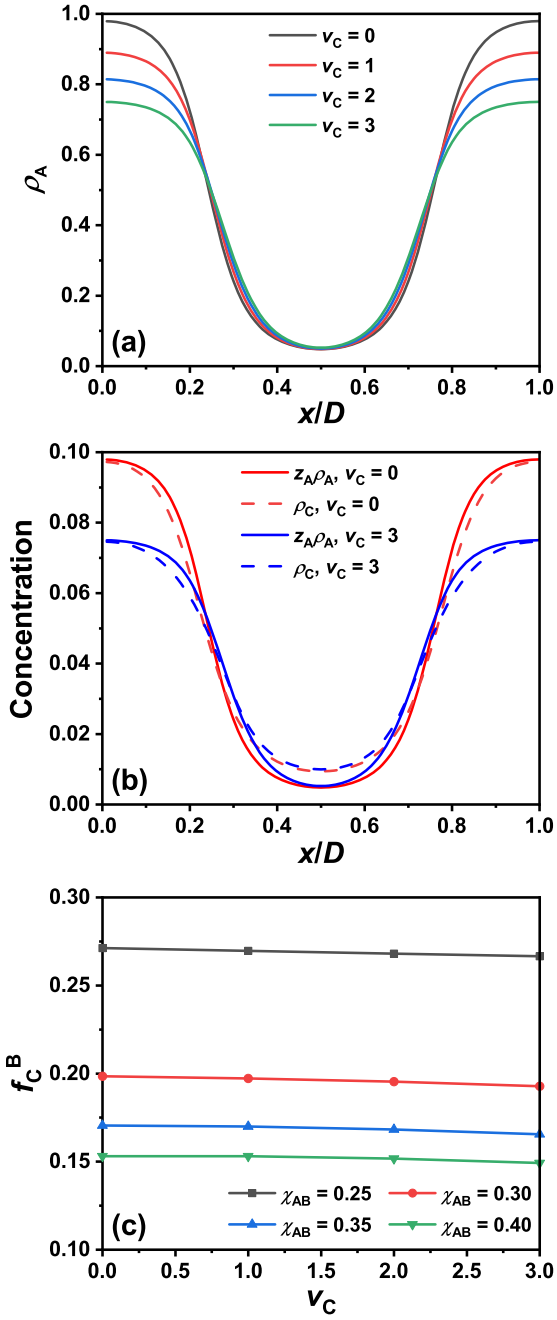

FIG. 4. Concentration distribution in L phase at different v_C with parameters f_A = 0.5 and χ_{AB} = 0.30. (a) Concentration distribution of monomer A (ρ_A). (b) Concentration of the charges on A blocks ($z_A\rho_A$) and counterions (ρ_C). (c) The fraction of counterions staying inside the B-rich domain as a function of counterion volume v_C at different incompatibility.

Obviously, the counterions are partially distributed in the B-rich domain and their translational entropy seems to be dominant. In Fig. 4(c), we give the fraction of counterions staying in the B-rich domain f_C^B, which is the ratio of the integration of counterion concentration within the B-rich region to the total counterion number within one period. As one can see, larger χ_{AB} leads to lower fraction of counterions in the B-rich region. Even for relative strong segregation $\chi_{AB}N$ = 40, ~15% of counterions remains in B-rich regions. Increasing the counterion size only decreases the fraction f_C^B slightly.

4. Counterions' distribution in H and G phases

It is believed that some complex phase, typically G phase, has a higher normalized ionic conductivity than other phase structures attributing to its structural advantages of continuous ionic channels.[20] Lin *et al.* also revealed that the inverse topology G and H phases are ideal candidates for solid-state electrolytes due to their optimal combination of high ion conductivity, well-percolated diffusion pathways, and mechanical robustness.[31] Therefore, to explore the morphological window of H and G phases as well as their formation mechanism is desirable for designing polyelectrolyte membranes with optimal performance. At the same time, to obtain the spatial distribution of counterions help us to understand the ion diffusion process. Matsen demonstrated that packing frustration in complex morphologies always occurs, and it results in strong stretching of part of chains in some regions, which plays an instrumental role in selection of complex phases.[61] For block copolymers, packing frustration leads to a tendency to form domains of uniform thickness so that none of the molecules are intensively stretched. However, adding homopolymers may relieve some packing frustration by filling the space of cell corners of the majority-component matrix and stabilize the complex phases.[62] Inspired by this idea, we want to reveal that whether there are some rules in our system to release the packing frustration by re-distribution of counterions. Take G phase and inverse H phase, for example, we know that polymer chains at different locations are stretched with varied degree in these two phases (see Fig. 5). Especially in the corner regions of each unit cell, the end part of the chain must be strongly stretched because of the constraint of spatial filling. This requirement means the great conformational entropy loss. A natural idea is that the packing frustration possibly drives the counterions with the excluded volume to be densely located in the red circle area (see Fig. 5)

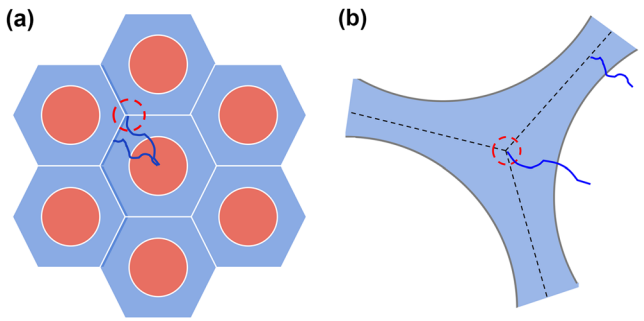

FIG. 5. Illustration of (a) inverse H phase and (b) G phase. In both (a) and (b), the gray continuous regions represent the A-rich region, the blue lines represents the polymer chain, and the red cycle areas represent the B-rich region. The counterions are accumulated in the A-rich region.

to release chain stretching and reduce the loss of conformational entropy.

The distributions of counterions in inverse H phase and G phase are shown in Fig. 6. Figures 6(a) and 6(e) are the sectional view for the concentration distribution of monomer A (ρ_A) and counterions C (ρ_C) for inverse H phase with parameters of χ_{AB} = 0.30, f_A = 0.68, v_C = 3, where the A monomers constitute the majority-component matrix. The redder the region, the greater the concentration in that region (the same below). The blue cycles here represent the columns formed by B-rich regions. Figures 6(a) and 6(b) have a similar pattern, indicating that the counterions are mainly concentrated in the A-rich region. The center region among three neighboring blue cylinders (forming a regular triangle) has the reddest color, indicating that the region has a high amount of counterions than that location in the middle point between two cylinders. Therefore, the enrichment of counterions in the corners of the hexagonal unit will reduce the chain stretching of the A block and relieve the packing frustration to some extent. However, this effect is not significant compared with the case of adding homopolymers[62] since the local volume fraction of counterions is only 0.07. We also calculated the relative concentration of counterions ρ_C^{rel} through $\rho_C^{rel} = \rho_C - z_A \times \rho_A$. The corresponding result is shown in Fig. 6(c). The reddest regions appear in the central area of cylinders, which are also the B-rich regions, indicating that partial counterions stay inside B-rich phases due to translational entropy.

We also consider the distributions of components in G phase with the A block as the minority component (f_A = 0.38). Similar phenomena can be observed [see Figs. 6(d), 6(e) and 6(f)]. The enrichment of counterions occurs in the region of the knots. Locally, the positive charges (A monomers) are almost compensated by negatively charged counterions. Thus, we conclude that in such a charged system, the packing frustration is not the main factor that impacts the distribution of counterions. The electrostatic interaction that causes the counterions to condense around the A blocks still plays a leading role. If the counterion has a larger excluded volume[19,42] or it is a charged surfactant,[63] this packing frustration effect possibly becomes important.

B. The effect of counterions' affinity

In above results, the counterions are assumed to have no preference to A or B blocks. In reality, counterions may have affinity to different blocks. Especially, if counterions have tendency to interact with B monomers, there is a competition between electrostatic attraction and preference with B blocks for the microphase-separated structure. The formed morphology as well as its properties will change significantly. It is believed that promoting charge dissociation is an important way to enhance the ionic conductivity in single-ion conducting systems. Ryu *et al.* found that incorporating the anions outside the ion-conducting

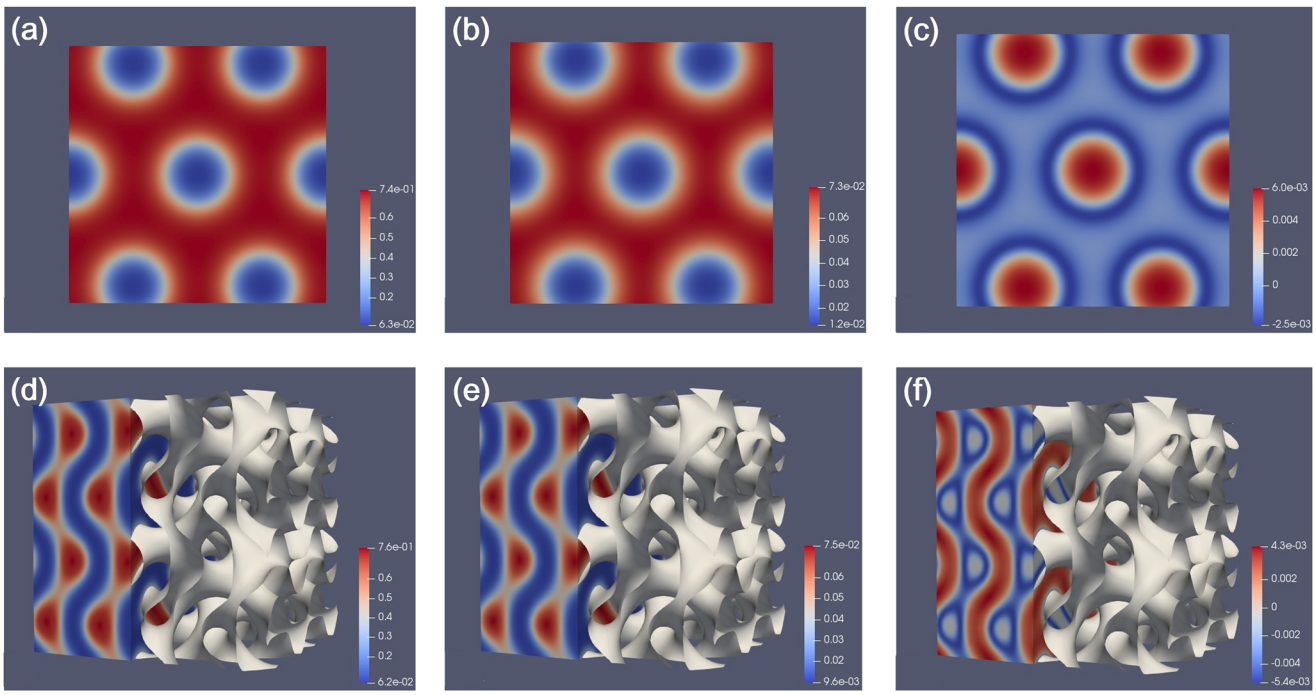

FIG. 6. Concentration distribution of (a) monomer A (ρ_A) and (b) counterions C (ρ_C) for inverse H phase. (c) Relative concentration of counterions ρ_C^{rel} for inverse H phase. ρ_C^{rel} is calculated by $\rho_C^{rel} = \rho_C - z_A \times \rho_A$ (the same below). For (a), (b), and (c), χ_{AB} = 0.30, f_A = 0.68, and v_C = 3. Concentration distribution of (d) monomer A (ρ_A) and (e) counterions C (ρ_C) for G phase. (f) Relative concentration of counterions ρ_C^{rel} for G phase. The white contours in (d), (e), and (f) show the channels in G phase. For (d), (e), and (f), χ_{AB} = 0.30, f_A = 0.38, and v_C = 3.

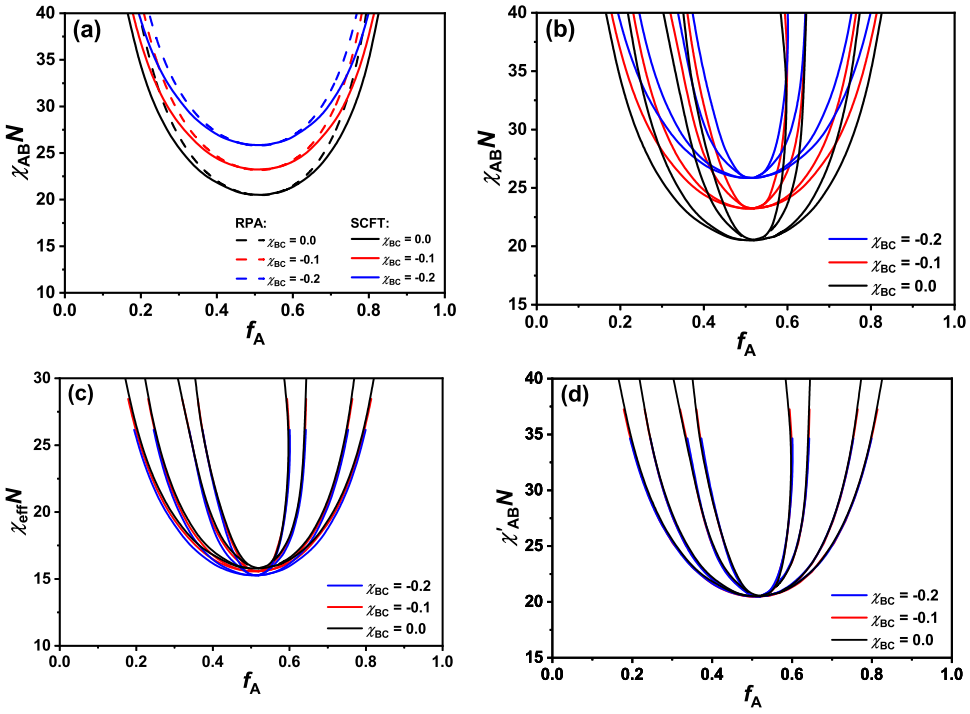

FIG. 7. The influence of counterion affinity on the phase diagram of neutral-charged diblock copolymers as a function of χ_{AB} and f_A with χ_{BC} = 0.0 (black), χ_{BC} = −0.1 (red), and χ_{BC} = −0.2 (blue). The charge fraction z_A = 0.1 and v_C = 3. (a) The comparison between stability limits (dashed curves) from the RPA and disorder-BCC phase boundaries (solid curves) from SCFT. (b) The phase diagram with L, H, G, and BCC phases at different χ_{BC} values. (c) The same phase diagram as in part (b) but with corrected incompatibility χ'_{AB}. (d) The shifted phase diagram for different affinities of χ_{BC}, the shift is completed by imposing χ'_{AB} at the critical point and is kept the same as χ_{BC} = 0.

block, such as in poly(lauryl methacrylate)-block-poly(lithium methacrylate)-block-poly[(oxyethylene)$_9$ methacrylate] (PLMA-b-PLiMA-b-POEM), could cause lithium ions to dissociate from the carboxylate counterions upon microphase separation of the POEM and PLMA blocks and thus enhance conductivity by two orders of magnitude compared with those incorporating anions into the conducting block.[9] Here, we consider the affinity effect of counterions to the two different blocks on the phase behavior. χ_{AC} and χ_{BC} reflect the affinity of the counterion to A and B blocks, respectively. A smaller χ_{BC} corresponds to larger affinity between counterions and the B block. In this section, v_C is set to 3.0 and χ_{AC} is fixed to 0.0 while varying χ_{BC} to see the effect of counterions' affinity.

Figure 7(a) gives the stability limits from RPA and ODT boundaries from SCFT with χ_{BC} = 0.0, −0.1, and −0.2, and it again shows a good agreement for results from two methods. The OOT phase diagram as a function of χ_{AB} and f_A is given in Fig. 7(b). With decreasing χ_{BC}, the phase diagram shifts upward as a whole. Therefore, a larger incompatibility between A and B blocks is required for microphase separation when counterion C has more preference with the B block, as one expected. Counterions are mainly bonded to the charged A blocks. The improvement of the affinity between counterions and the B block results in enrichment of counterions within B-rich domains, which inevitably cause more A chains staying with B blocks, given that the electrostatic interaction plays a role. Consequently, to increase the affinity of counterions to B improves effectively the compatibility between A and B blocks, and a larger separation strength between A and B blocks is required for microphase separation. Figure 8 gives the concentration distributions of monomer A and counterion C in a typical L phase at

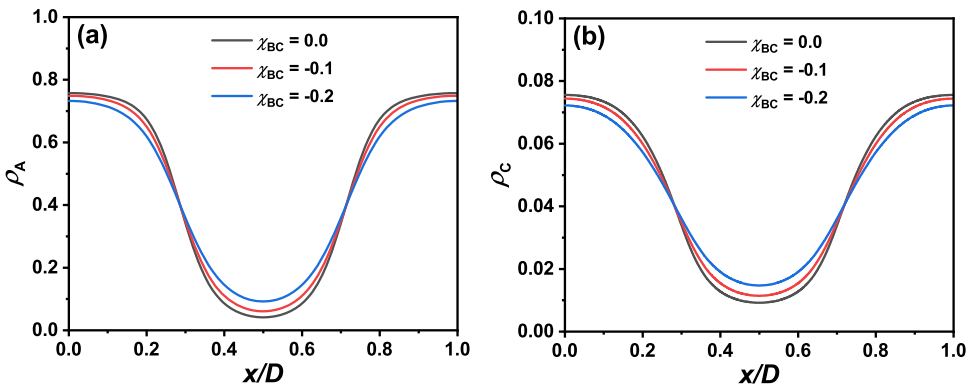

FIG. 8. Concentration distribution in L phase at different χ_{BC} with parameters f_A = 0.52 and χ_{AB} = 0.32. (a) Concentration distribution of monomer A (ρ_A). (b) Concentration of counterions (ρ_C).

different χ_{BC} with parameters $f_A = 0.52$ and $\chi_{AB} = 0.32$. It shows that decreasing χ_{BC} gives rise to the increase in amounts of both monomer A and counterion C in the B block domain. At the same time, the A/B interface becomes more smooth. We conclude that improvement of affinity between the B block and counterion C can enhance the degree of charge dissociation in single-ion conducting systems.

It is noted that the OOT boundaries for different χ_{BC} have very similar shape. Thus, we speculate that the complex role of χ_{BC} may probably be described using an effective χ parameter between A and B monomers through $\chi_{eff} = (\chi_{AB} + z_A v_C \chi_{BC})/(1 + z_A v_C)$, which formula assumes that all counterions are uniformly distributed in the A-rich region. The corrected phase diagram is shown in Fig. 7(c). One can see good agreement after correction using χ_{eff}. However, recognizable difference still exists for the bottom part since partial counterions have to stay inside the B-rich phase, which means that the translational entropy of counterions is also important. In order to eliminate the difference and deduce the role of counterion affinity, we re-plot the phase diagrams by using a, namely, χ'_{AB} parameter for $\chi_{BC} < 0$. We move down the phase boundaries of the system with $\chi_{BC} = -0.1$ (red curves) and $\chi_{BC} = -0.2$ (blue curves) to make all critical points (corresponding to $f_A = 0.53$) overlapped. By doing this, all phase boundaries with different χ_{BC} can be almost normalized to one with $\chi_{BC} = 0$, as shown in Fig. 7(a). Based on the above results, we found that the affinity effect of counterions χ_{BC} can be mapped into an effective incompatibility parameter as $\chi'_{AB} = \chi_{AB} + 0.27\chi_{BC}$ in the present case of $\chi_{AC} = 0$.

IV. CONCLUSION

In this article, using RPA and SCFT, we systematically investigate the effect of counterions' size and affinity on phase behavior in neutral-charged diblock copolymer melts for the first time. The phase diagrams as a function of χ_{AB} and f_A with different counterions' sizes is constructed first. Increasing counterions' size causes the phase diagram to shift upward and leftward, which is attributed to electrostatic interactions and the intrinsic volume of counterions. The movement of phase boundaries is more obvious for the system with the major A component ($f_A > 0.5$) compared to that with the minor A component. We then display the domain spacing of ordered phase as a function of χ_{AB} or f_A. The domain spacing in such a system shows an unexpected tendency that it decreases with increasing counterions' size, which is due to the increased miscibility between A/B domains induced by larger counterions. The interfacial width of the L phase is then calculated, and a good linear dependence between the interface width and counterions' size is observed. We further calculate the concentration distributions of monomer A and counterion in the typical L phase. The results show that increasing counterion size gives rise to the densities of both monomer A and counterions in the A-rich region. However, there are still partial counterions staying in the B-rich region, and the proportion is almost independent of counterion size. The counterions' distributions in H and G phases demonstrate that it is electrostatic interaction, instead of packing frustration, playing a leading role in such systems. The phase diagrams at different counterions' affinities are also constructed. The improvement of affinity between counterions and B block results in upward shifts of the phase diagram. The concentration distributions reveal that smaller χ_{BC} (larger affinity to the B block) gives rise to the enrichment of counterions in the B domain, which consequently leads to a better miscibility between A/B blocks. Furthermore, in our case, the affinity effect can be mapped into an effective $\chi'_{AB} = \chi_{AB} + 0.27\chi_{BC}$. We demonstrate that increasing the affinity between counterions and the B block can exactly enhance the miscibility between two blocks, which may become an effective method in designing a polyelectrolyte membrane with higher conductivity. This work may provide a fundamental understanding about counterions and a useful guidance in the construction of desired nanostructures of block polyelectrolytes with improved properties.

ACKNOWLEDGMENTS

The authors acknowledge the financial support from the National Natural Science Foundation of China (NSFC) (Grant Nos. 21674005, 21634001, and 21474005).

REFERENCES

[1] F. S. Bates and G. H. Fredrickson, "Block copolymers—Designer soft materials," Phys. Today **52**(2), 32–38 (1999).
[2] D. Golodnitsky, E. Strauss, E. Peled, and S. Greenbaum, "Review-on order and disorder in polymer electrolytes," J. Electrochem. Soc. **162**, A2551–A2566 (2015).
[3] D. T. Hallinan and N. P. Balsara, "Polymer electrolytes," Annu. Rev. Mater. Res. **43**, 503–525 (2013).
[4] C. Park, J. Yoon, and E. L. Thomas, "Enabling nanotechnology with self assembled block copolymer patterns," Polymer **44**, 6725–6760 (2003).
[5] W.-S. Young, P. J. Brigandi, and T. H. Epps III, "Crystallization-induced lamellar-to-lamellar thermal transition in salt-containing block copolymer electrolytes," Macromolecules **41**, 6276–6279 (2008).
[6] W.-S. Young and T. H. Epps III, "Salt doping in peo-containing block copolymers: Counterion and concentration effects," Macromolecules **42**, 2672–2678 (2009).
[7] M. Singh, O. Odusanya, G. M. Wilmes, H. B. Eitouni, E. D. Gomez, A. J. Patel, V. L. Chen, M. J. Park, P. Fragouli, H. Iatrou, N. Hadjichristidis, D. Cookson, and N. P. Balsara, "Effect of molecular weight on the mechanical and electrical properties of block copolymer electrolytes," Macromolecules **40**, 4578–4585 (2007).
[8] A. Panday, S. Mullin, E. D. Gomez, N. Wanakule, V. L. Chen, A. Hexemer, J. Pople, and N. P. Balsara, "Effect of molecular weight and salt concentration on conductivity of block copolymer electrolytes," Macromolecules **42**, 4632–4637 (2009).
[9] S.-W. Ryu, P. E. Trapa, S. C. Olugebefola, J. A. Gonzalez-Leon, D. R. Sadoway, and A. M. Mayes, "Effect of counter ion placement on conductivity in single-ion conducting block copolymer electrolytes," J. Electrochem. Soc. **152**, A158–A163 (2005).
[10] D. R. Sadoway, B. Huang, P. E. Trapa, P. P. Soo, P. Bannerjee, and A. M. Mayes, "Self-doped block copolymer electrolytes for solid-state, rechargeable lithium batteries," J. Power Sources **97-98**, 621–623 (2001).
[11] H. Mazor, D. Golodnitsky, E. Peled, W. Wieczorek, and B. Scrosati, "A search for a single-ion-conducting polymer electrolyte: Combined effect of anion trap and inorganic filler," J. Power Sources **178**, 736–743 (2008).
[12] R. Bouchet, S. Maria, R. Meziane, A. Aboulaich, L. Lienafa, J.-P. Bonnet, T. N. T. Phan, D. Bertin, D. Gigmes, D. Devaux, R. Denoyel, and M. Armand, "Single-ion BAB triblock copolymers as highly efficient electrolytes for lithium-metal batteries," Nat. Mater. **12**, 452–457 (2013).
[13] A. A. Rojas, S. Inceoglu, N. G. Mackay, J. L. Thelen, D. Devaux, G. M. Stone, and N. P. Balsara, "Effect of lithium-ion concentration on morphology and ion transport in single-ion-conducting block copolymer electrolytes," Macromolecules **48**, 6589–6595 (2015).

[14]M. Watanabe and A. Nishimoto, "Effects of network structures and incorporated salt species on electrochemical properties of polyether-based polymer electrolytes," Solid State Ionics **79**, 306–312 (1995).
[15]G. B. Appetecchi, D. Zane, and B. Scrosati, "PEO-based electrolyte membranes based on $LiBC_4O_8$ salt," J. Electrochem. Soc. **151**, A1369–A1374 (2004).
[16]K. E. Thomas, S. E. Sloop, J. B. Kerr, and J. Newman, "Comparison of lithium-polymer cell performance with unity and nonunity transference numbers," J. Power Sources **89**, 132–138 (2000).
[17]C. Monroe and J. Newman, "Dendrite growth in lithium/polymer systems—A propagation model for liquid electrolytes under galvanostatic conditions," J. Electrochem. Soc. **150**, A1377–A1384 (2003).
[18]X. Wang, M. Goswami, R. Kumar, B. G. Sumpter, and J. Mays, "Morphologies of block copolymers composed of charged and neutral blocks," Soft Matter **8**, 3036–3052 (2012).
[19]H. Y. Jung, S. Y. Kim, O. Kim, and M. J. Park, "Effect of the protogenic group on the phase behavior and ion transport properties of acid-bearing block copolymers," Macromolecules **48**, 6142–6152 (2015).
[20]G. Jo, H. Ahn, and M. J. Park, "Simple route for tuning the morphology and conductivity of polymer electrolytes: One end functional group is enough," ACS Macro Lett. **2**, 990–995 (2013).
[21]S. Inceoglu, A. A. Rojas, D. Devaux, X. C. Chen, G. M. Stone, and N. P. Balsara, "Morphology-conductivity relationship of single-ion-conducting block copolymer electrolytes for lithium batteries," ACS Macro Lett. **3**, 510–514 (2014).
[22]Y. Rabin and J. F. Marko, "Microphase separation in charged diblock copolymers: The weak segregation limit," Macromolecules **24**, 2134–2136 (1991).
[23]J. F. Marko and Y. Rabin, "Microphase separation of charged diblock copolymers: Melts and solutions," Macromolecules **25**, 1503–1509 (1992).
[24]R. Kumar and M. Muthukumar, "Microphase separation in polyelectrolytic diblock copolymer melt: Weak segregation limit," J. Chem. Phys. **126**, 214902 (2007).
[25]S. Yang, A. Vishnyakov, and A. V. Neimark, "Self-assembly in block polyelectrolytes," J. Chem. Phys. **134**, 054104 (2011).
[26]L. Wang, J. Lin, and Q. Zhang, "Self-consistent field theory study of the solvation effect in polyelectrolyte solutions: Beyond the Poisson-Boltzmann model," Soft Matter **9**, 4015–4025 (2013).
[27]Y.-X. Liu, H.-D. Zhang, C.-H. Tong, and Y.-L. Yang, "Microphase separation and phase diagram of concentrated diblock copolyelectrolyte solutions studied by self-consistent field theory calculations in two-dimensional space," Macromolecules **44**, 8261–8269 (2011).
[28]C. E. Sing, J. W. Zwanikken, and M. O. de la Cruz, "Theory of melt polyelectrolyte blends and block copolymers: Phase behavior, surface tension, and microphase periodicity," J. Chem. Phys. **142**, 034902 (2015).
[29]C. E. Sing, J. W. Zwanikken, and M. O. de la Cruz, "Electrostatic control of block copolymer morphology," Nat. Mater. **13**, 694–698 (2014).
[30]M. Radhakrishna and C. E. Sing, "Charge correlations for precise, coulombically driven self assembly," Macromol. Chem. Phys. **217**, 126–136 (2016).
[31]C. Zhai, H. Zhou, T. Gao, L. Zhao, and S. Lin, "Electrostatically tuned microdomain morphology and phase-dependent ion transport anisotropy in single-ion conducting block copolyelectrolytes," Macromolecules **51**, 4471–4483 (2018).
[32]Z.-G. Wang, "Effects of ion solvation on the miscibility of binary polymer blends," J. Phys. Chem. B **112**, 16205–16213 (2008).
[33]I. Nakamura, N. P. Balsara, and Z.-G. Wang, "Thermodynamics of ion-containing polymer blends and block copolymers," Phys. Rev. Lett. **107**, 198301 (2011).
[34]I. Nakamura and Z.-G. Wang, "Salt-doped block copolymers: Ion distribution, domain spacing and effective chi parameter," Soft Matter **8**, 9356–9367 (2012).
[35]I. Nakamura, N. P. Balsara, and Z.-G. Wang, "First-order disordered-to-lamellar phase transition in lithium salt-doped block copolymers," ACS Macro Lett. **2**, 478–481 (2013).
[36]K. J. Hou and J. Qin, "Solvation and entropic regimes in ion-containing block copolymers," Macromolecules **51**, 7463–7475 (2018).
[37]W. Chu, J. Qin, and J. J. de Pablo, "Ion distribution in microphase-separated copolymers with periodic dielectric permittivity," Macromolecules **51**, 1986–1991 (2018).
[38]D. J. Grzetic, K. T. Delaney, and G. H. Fredrickson, "Field-theoretic study of salt-induced order and disorder in a polarizable diblock copolymer," ACS Macro Lett. **8**, 962–967 (2019).
[39]J. R. Brown, Y. Seo, and L. M. Hall, "Ion correlation effects in salt-doped block copolymers," Phys. Rev. Lett. **120**, 127801 (2018).
[40]Y.-L. Zhu, Z.-Y. Lu, G. Milano, A.-C. Shi, and Z.-Y. Sun, "Hybrid particle-field molecular dynamics simulation for polyelectrolyte systems," Phys. Chem. Chem. Phys. **18**, 9799–9808 (2016).
[41]T. M. Bennett, L. C. Chambers, K. J. Thurecht, K. S. Jack, and I. Blakey, "Dependence of block copolymer domain spacing and morphology on the cation structure of ionic liquid additives," Macromolecules **51**, 8979–8986 (2018).
[42]C. Iacob, A. Matsumoto, M. Brennan, H. Liu, S. J. Paddison, O. Urakawa, T. Inoue, J. Sangoro, and J. Runt, "Polymerized ionic liquids: Correlation of ionic conductivity with nanoscale morphology and counterion volume," ACS Macro Lett. **6**, 941–946 (2017).
[43]E. Ji, V. Pellerin, L. Rubatat, E. Grelet, A. Bousquet, and L. Billon, "Self-assembly of ionizable "clicked" P3HT-*b*-PMMA copolymers: Ionic bonding group/counterion effects on morphology," Macromolecules **50**, 235–243 (2017).
[44]R.-Y. Wang, X.-S. Guo, B. Fan, S.-F. Zou, X.-H. Cao, Z.-Z. Tong, J.-T. Xu, B.-Y. Du, and Z.-Q. Fan, "Design and regulation of lower disorder-to-order transition behavior in the strongly interacting block copolymers," Macromolecules **51**, 2302–2311 (2018).
[45]A. Dehghan, M. Schick, and A.-C. Shi, "Effect of mobile ions on the electric field needed to orient charged diblock copolymer thin films," J. Chem. Phys. **143**, 134902 (2015).
[46]W. S. Loo, M. D. Galluzzo, X. Li, J. A. Maslyn, H. J. Oh, K. I. Mongcopa, C. Zhu, A. A. Wang, X. Wang, B. A. Garetz, and N. P. Balsara, "Phase behavior of mixtures of block copolymers and a lithium salt," J. Phys. Chem. B **122**, 8065–8074 (2018).
[47]I. Nakamura and Z.-G. Wang, "Thermodynamics of salt-doped block copolymers," ACS Macro Lett. **3**, 708–711 (2014).
[48]S. L. Bore, H. B. Kolli, T. Kawakatsu, G. Milano, and M. Cascella, "Mesoscale electrostatics driving particle dynamics in nonhomogeneous dielectrics," J. Chem. Theory Comput. **15**, 2033–2041 (2019).
[49]H. B. Kolli, A. de Nicola, S. L. Bore, K. Schäfer, G. Diezemann, J. Gauss, T. Kawakatsu, Z.-Y. Lu, Y.-L. Zhu, G. Milano, and M. Cascella, "Hybrid particle-field molecular dynamics simulations of charged amphiphiles in an aqueous environment," J. Chem. Theory Comput. **14**, 4928–4937 (2018).
[50]L. Leibler, "Theory of microphase separation in block copolymers," Macromolecules **13**, 1602–1617 (1980).
[51]T. A. Vilgis, M. Benmouna, and H. Benoit, "Static scattering from multicomponent polymer systems: Theoretical models," Macromolecules **24**, 4481–4488 (1991).
[52]A.-C. Shi and J. Noolandi, "Theory of inhomogeneous weakly charged polyelectrolytes," Macromol. Theory Simul. **8**, 214–229 (1999).
[53]G. H. Fredrickson, *The Equilibrium Theory of Inhomogenous Polymers* (Oxford Science Publications, 2006).
[54]M. W. Matsen and M. Schick, "Stable and unstable phases of a diblock copolymer melt," Phys. Rev. Lett. **72**, 2660–2663 (1994).
[55]H. Bai, *Authoritative Guide on FORTRAN Program Designing* (China Machine Press, 2013).
[56]N. Kin-Chue, "Hypernetted chain solutions for the classical one-component plasma up to Γ = 7000," J. Chem. Phys. **61**, 2680–2689 (1974).
[57]M. W. Matsen, "Fast and accurate scft calculations for periodic block-copolymer morphologies using the spectral method with Anderson mixing," Eur. Phys. J. E **30**, 361–369 (2009).

[58]R. B. Thompson, K. O. Rasmussen, and T. Lookman, "Improved convergence in block copolymer self-consistent field theory by Anderson mixing," J. Chem. Phys. **120**, 31–34 (2004).
[59]M. W. Matsen, "The standard Gaussian model for block copolymer melts," J. Phys.: Condens. Matter **14**, R21–R47 (2002).
[60]M. W. Matsen and R. B. Thompson, "Equilibrium behavior of symmetric ABA triblock copolymer melts," J. Chem. Phys. **111**, 7139–7146 (1999).
[61]M. W. Matsen and F. S. Bates, "Origins of complex self-assembly in block copolymers," Macromolecules **29**, 7641–7644 (1996).
[62]M. W. Matsen, "Phase-behavior of block-copolymer homopolymer blends," Macromolecules **28**, 5765–5773 (1995).
[63]J. M. Borreguero, P. A. Pincus, B. G. Sumpter, and M. Goswami, "Unraveling the agglomeration mechanism in charged block copolymer and surfactant complexes," Macromolecules **50**, 1193–1205 (2017).